Biogeosciences Discuss., 10, 7031–7074, 2013
www.biogeosciences-discuss.net/10/7031/2013/
doi:10.5194/bgd-10-7031-2013

Biogeosciences
Discussions
Open Access

Seasonal variations of air-sea CO_2 fluxes in the largest tropical marginal sea (South China Sea) based on multiple-year underway measurements

W.-D. Zhai[1,2], M.-H. Dai[1], B.-S. Chen[1,3], X.-H. Guo[1], Q. Li[1], S.-L. Shang[1], C.-Y. Zhang[1], W.-J. Cai[3,4], and D.-X. Wang[5]

[1]State Key Laboratory of Marine Environmental Science, Xiamen University, Xiamen 361005, China
[2]National Marine Environmental Monitoring Center, Dalian 116023, China
[3]Department of Marine Sciences, University of Georgia, Athens, GA 30602, USA
[4]School of Marine Science and Policy, University of Delaware, Newark, DE 19716, USA
[5]State Key Laboratory of Tropical Oceanography, South China Sea Institute of Oceanology, Chinese Academy of Sciences, Guangzhou 510301, China

Received: 27 March 2013 – Accepted: 10 April 2013 – Published: 19 April 2013

Correspondence to: M.-H. Dai (mdai@xmu.edu.cn)

Published by Copernicus Publications on behalf of the European Geosciences Union.

Seasonal variations of air-sea CO_2 fluxes in the South China Sea

W.-D. Zhai et al.

Abstract

Based upon fourteen field surveys conducted between 2003 and 2008, we showed that the seasonal pattern of sea surface partial pressure of CO_2 (pCO_2) and air–sea CO_2 fluxes differed among four different physical-biogeochemical domains in the South China Sea (SCS) proper. The four domains were located between 4 and 23° N and 109 and 121° E, covering ~38 % of the surface area of the entire SCS. In the area off the Pearl River Estuary, relatively low pCO_2 values of 320 to 390 µatm were observed in all four seasons and both the biological productivity and CO_2 uptake were enhanced in summer in the Pearl River plume waters. In the northern SCS slope/basin area, a typical seasonal cycle of relatively high pCO_2 in the warmer seasons and relatively low pCO_2 in the cold seasons was revealed. In the central/southern SCS area, moderately high sea surface pCO_2 values of 360 to 425 µatm were observed throughout the year. In the area west of the Luzon Strait, a major exchange pathway between the SCS and the Pacific Ocean, pCO_2 was particularly dynamic in winter, when northeast monsoon induced upwelling events and strong outgassing of CO_2. These episodic events might have dominated the annual air–sea CO_2 flux in this particular area. The estimate of annual sea–air CO_2 fluxes showed that, most areas of the SCS proper served as weak sources to the atmospheric CO_2, with sea–air CO_2 flux values of $0.46 \pm 0.43\,\mathrm{mol\,m^{-2}\,yr^{-1}}$ in the northern SCS slope/basin, $1.37 \pm 0.55\,\mathrm{mol\,m^{-2}\,yr^{-1}}$ in the central/southern SCS, and $1.21 \pm 1.47\,\mathrm{mol\,m^{-2}\,yr^{-1}}$ in the area west of the Luzon Strait. However, the annual sea–air CO_2 exchange was nearly in equilibrium ($-0.44 \pm 0.65\,\mathrm{mol\,m^{-2}\,yr^{-1}}$) in the area off the Pearl River Estuary. Overall the four domains released $(18 \pm 10) \times 10^{12}\,\mathrm{g\,C\,yr^{-1}}$ into the atmosphere. The CO_2 release rate of the South China Sea essentially exceeded the average CO_2 emission level of most tropical oceans.

BGD

10, 7031–7074, 2013

1 Introduction

As an important component of global carbon cycling, coastal ocean carbon has received considerable attention during the past three decades (e.g. Walsh et al., 1981; Smith and Hollibaugh, 1993; Tsunogai et al., 1999; Borges et al., 2005; Cai et al., 2006; Chen and Borges, 2009; Laruelle et al., 2010; Liu et al., 2010; Borges, 2011; Cai, 2011; Dai et al., 2013). Recent estimates of global coastal ocean sea–air CO_2 fluxes have converged to conclude that the coastal ocean is an atmospheric CO_2 sink of 0.2 to 0.4 $\mathrm{Pg\,C\,yr^{-1}}$ (Cai et al., 2006; Chen and Borges, 2009; Laruelle et al., 2010; Liu et al., 2010; Borges, 2011; Cai, 2011; Dai et al., 2013). This current estimate is a significant change from the earlier speculation of up to 1 $\mathrm{Pg\,C\,yr^{-1}}$ (Tsunogai et al., 1999); but confirms that the coastal ocean plays a disproportionally important role in the global ocean carbon budget.

It must be pointed out that the above compilation of the global scale air–sea CO_2 fluxes in the coastal ocean is often based on snap-shot measurements in individual systems. In many of these coastal systems, spatial and temporal changes in CO_2 fluxes remain to be resolved as large uncertainties are often associated with the presently reported CO_2 fluxes in individual coastal ocean system, which would in turn impact on the estimation of global fluxes. From the perspective of predictability of future change, both the variation in time and space as well as the inherent controlling processes need to be better understood. Adding even more complexity is that the coastal ocean is very often characterized by the highest spatial gradient in both physics and biogeochemistry, and hence has inherited complicated and differing physical-biogeochemical domains.

The South China Sea (SCS) is such a marginal sea system encompassing a large variety of physical-biogeochemical domains. The SCS proper, located between 4 and 23° N and 109 and 121° E and characterized by either a tropical or subtropical climate, has both deep basins and extensive shelf systems in the northern and southern boundaries (Fig. 1) associated with large riverine inputs. The SCS is also featured by dynamic exchange with the West Pacific Ocean, via an upper part exchange with the

BGD
10, 7031–7074, 2013

Kuroshio and overflow at depth (Chen et al., 2001). At this dynamic interface, meso-scale processes such as eddies are frequently observable. As such, enriched physical-biogeochemical domains are concentrated in the SCS (Fig. 1), which also represents the lines of the present study. We considered four contrasting physical-biogeochemical domains, and were able to significantly improve our understanding regarding the spatial variability of CO_2 fluxes. Besides our multiple-year measurements, we were much better positioned to provide CO_2 fluxes in the SCS at a resolution of seasonal levels. Among these four domains, A was adjacent to the Pearl River Estuary (PRE) and was thus influenced by the summer estuarine plume (Gan et al., 2009; Cao et al., 2010; Han et al., 2012). Domain B covered the slope and deep basin areas in the northern SCS, which is typically oligotrophic (Wong et al., 2007) and low in productivity (Chen and Chen, 2006). Domain C covered a large portion of the SCS basin and is characterized by a tropical oligotrophic environment (Ning et al., 2004). Domain D was located west of the Luzon Strait and was impacted by the Kuroshio intrusions which generate various meso-scale eddies and internal waves (e.g. Li et al., 1998; Yuan et al., 2006; Chen et al., 2007a; Sheu et al., 2010a).

Thus far, limited datasets with different spatial coverage have suggested that the SCS proper serves as a weak or moderate source of atmospheric CO_2 in warm seasons (Rehder and Suess, 2001; Zhai et al., 2005a, 2009). Based on a summary of limited carbonate system data from the late 1990s and mass balance calculations, Chen et al. (2006) suggest that the SCS is overall a very weak CO_2 source. In contrast, based on time series observations at the SEATS (Southeast Asian Time Series Study) station (18° 15′ N, 115° 35′ E), Chou et al. (2005), Tseng et al. (2007), and Sheu et al. (2010b) note seasonal and inter-annual variabilities of carbon chemistry including computed surface $p CO_2$ between December 1999 and December 2008, and report that the northern SCS serves as a weak sink of atmospheric CO_2 by extrapolating the SEATS results to the entire region. We note that previous estimates of annual air–sea CO_2 fluxes in the SCS proper are either based on limited transects/stations (Zhai et al., 2005a; Chen et al., 2006), or even spatially extrapolated from time-series observations at a single site (Chou et al., 2005; Tseng et al., 2007; Sheu et al., 2010b). We contend that this limited spatial coverage has hampered the better assessment of pCO$_2$ variability in the SCS (Fig. 1). In our study, we greatly improved the current coverage by applying a large amount of new datasets obtained from multiple years and large-scale underway surveys (Fig. 2), extending our mechanistic understanding of pCO$_2$ variability in this important tropical marginal sea, which is necessary before placing the SCS CO_2 flux in a global context.

2 Study area

The SCS proper in this study is bounded by the China mainland on the north and northwest sides, Vietnam on the west and southwest sides, the Sunda Shelf and Borneo on the south side, Taiwan Island on the northeast side and the Philippines on the east side (Fig. 1). In its northern part, climatic variations of the air–sea interface are primarily dominated by the Asian Monsoon. The rain-bearing southwest monsoon lasts from June to September, but the northeast monsoon, typically with higher wind speed prevails in winter, from November to March (Han, 1998).

The center of the SCS proper is a deep basin with a maximum depth exceeding 4700 m, which is surrounded by extensive shelf systems in the northern and southern boundaries. In the east and west boundaries, however, the shelves are narrow and the slopes are steep. The SCS proper has a basin wide cyclonic gyre in the winter and an anticylonic gyre over the southern half in the summer. The latter is usually associated with an eastward jet off the coast of Vietnam (Fig. 1). The northern SCS also exchanges with the Kuroshio via the Luzon Strait of 2000 m depth. Although the SCS shelf systems are fed by two of the world's major rivers (the Mekong and the Pearl River) and some smaller rivers featuring either tropical or subtropical watersheds, the majority of the SCS proper is typically oligotrophic with low productivity (Ning et al., 2004; Chen and Chen, 2006). In our study, we focused on four physical-biogeochemical domains in the SCS proper (Fig. 1; Table 1).

BGD
10, 7031–7074, 2013

Among the four domains, A could absorb CO_2 from the atmosphere in the spring/summer bloom periods (Dai et al., 2008; Zhai et al., 2009; Cao et al., 2011), while during the northeast monsoon seasons it was influenced by the cooling effect and intrusion of the Kuroshio (Fig. 1). Domain B was located between 18 and 21° N and 112 and 118° E. Zhai et al. (2005a) suggest that most of the sea surface partial pressure of CO_2 (pCO_2) in this domain is dependent on sea surface temperature (SST), and this varies around $(370 \pm 20\,\mu\text{atm}) \times e^{0.0423(\text{SST}-26)}$. Domain C was located between 7 and 18° N and 110 and 117° E. As the deep basin of the SCS, its upper mixed layer is shallow all the year round. Both meso-scale eddies and the Mekong River plume have impacts on the southwestern part of this domain during the southwest monsoon period (e.g. Chen et al., 2010; Hu et al., 2011). However, regionally averaged primary production and sea surface chlorophyll concentrations vary within limited ranges (Tan and Shi, 2009; Sasai et al., 2013). On the other hand, due to abundant coral reefs on Nansha, Xisha and Zhongsha Islands, this domain was potentially influenced by $CaCO_3$ formation, which releases CO_2 into the atmosphere (Dai et al., 2009; Yan et al., 2011). Domain D was located between 18 and 21° N and 118 and 121° E, where the Kuroshio intrusions generate meso-scale cyclonic eddies in the northeast monsoon season (Sheu et al., 2010a) and thus induce pumping/entrainment of nutrients and CO_2 from the depths (e.g. Xu et al., 2009; Shang et al., 2012; Sasai et al., 2013). The total area of the four domains was estimated as $1344 \times 10^3\,\text{km}^2$, accounting for the majority of the SCS proper (Fig. 1) and 38 % of the total area of the SCS.

3 Sampling and methods

Between October 2003 and April 2008, 14 cruises (Table 2) were made aboard R/V *Shiyan 3* (October 2003, May 2004 and September 2004), R/V *Yanping 2* (February 2004 and July 2004), R/V *Haijian 83* (February 2006), R/V *Kexue 3* (October 2006) and R/V *Dongfanghong 2* (the rest). During these cruises, except for September 2004,

BGD
10, 7031–7074, 2013

Seasonal variations of air-sea CO_2 fluxes in the South China Sea

W.-D. Zhai et al.

quasi-surface water was continuously pumped into instruments for analysis from a side intake at a depth of 2 to 3 m (for R/V *Yanping 2* and R/V *Kexue 3*) or 4 to 5 m (for R/V *Shiyan* 3, R/V *Haijian 83* and R/V *Dongfanghong 2*). During the September 2004 survey, surface water at 0.5 to 1 m depth was pumped up and measured for 30 min at every station. On February 2006, a parallel study was carried out at and around the Xisha Islands (Dai et al., 2009), and the data measured underway (5 to 10 nautical miles off the Islands) are also plotted in Fig. 2b. During the continuous/discrete pumping, the temperature, salinity and $p\mathrm{CO_2}$ of the seawater were continuously measured and recorded. Note the July 2004 cruise has been described in Zhai et al. (2009). And some of the data collected in February 2004 have been reported in Jo et al. (2012). See Table 2 for details.

3.1 Temperature and salinity determination

During the cruises, the temperature and salinity of the pumped seawater were continuously measured using a SEACAT thermosalinograph system (CTD, SBE21, Sea-Bird Co., USA) (February 2004 and July 2004), or a set of Idronaut Multiparameter "Flow Through" sensor modules (IDRONAUT S.r.l., Italy) (April 2008), or a YSI 6600 meter (Yellow Springs Instrument Co., USA) (the other cruises). All salinity data were corrected to the practical salinity scale 1978 by inter-calibration testing either shortly before or during the cruises. Also based on these inter-calibration tests, we estimated that all the onboard temperature sensors were consistent with the others at an error level of less than 0.1 °C. During most cruises, other than the February 2004, July 2004 and September 2004 cruises, SST was calculated via on-board temperature minus 0.2 °C (in cool surveys) or 0.3 °C (in warm surveys) based on inter-comparison experiments between underway pumping measurements and vertical profile measurements at the stations. During the February 2004 and July 2004 cruises, however, SST was continuously measured using the in situ temperature sensor of the SBE21 system. During the September 2004 cruise, SST was discretely measured using another

BGD
10, 7031–7074, 2013

Seasonal variations of air-sea CO_2 fluxes in the South China Sea

W.-D. Zhai et al.

Title Page
Abstract | Introduction
Conclusions | References
Tables | Figures
◀| |▶
◀ ▶
Back | Close
Full Screen / Esc
Printer-friendly Version
Interactive Discussion

SEACAT thermosalinograph system (SBE911+, Sea-Bird Co., USA) at every station. All the continuous data were recorded every 6 to 12 s and averaged to 1 min.

3.2 Meteorological data

Meteorological data (wind speed, wind direction and barometric pressure) were collected with an onboard weather station at 10 m above the sea surface. Data were recorded every minute. For the purpose of flux calculation, satellite-derived monthly mean wind speeds (QuikSCAT, Level 3, http://podaac.jpl.nasa.gov) referenced at 10 m above the sea surface were used. The monthly mean wind speed data for a specific domain was calculated by averaging all of the available wind speed data for the month.

3.3 $p\mathrm{CO_2}$ determination

During most cruises, other than the April 2008 cruise, improved systems after Zhai et al. (2005b) and/or Jiang et al. (2008) were used to measure $p\mathrm{CO_2}$. During our April 2008 cruise, an automated flowing $p\mathrm{CO_2}$ measuring system (GO8050, General Oceanics Inc., USA) was used (Zhai and Dai, 2009). In these systems, a Li-Cor® non-dispersive infrared spectrometer (Li-6252 during the October 2003 and May 2004 surveys, Li-7000 during the other cruises) was used to measure dried $\mathrm{CO_2}$ fractions ($x\mathrm{CO_2}$) in the equilibrator and in the air (Zhai et al., 2005b; Zhai and Dai, 2009). For calibration purposes, a series of $\mathrm{CO_2}$ gas standards with $x\mathrm{CO_2}$ values from 138 to 967 ppmv (parts per million volumes in dry air; the same hereafter) were applied. $p\mathrm{CO_2}$ was transformed from corrected $x\mathrm{CO_2}$ based on air pressure along the transect or barometric pressure around the Li-7000 detector. Inter-calibration testing showed that both air pressure datasets were consistent at a relative error level of less than 0.3 % (i.e. <3 hPa). The Weiss and Price (1980) saturated water vapor pressure and the Takahashi et al. (1993) temperature effect coefficient of 4.23 % °C^{-1} were used to calculate the in situ $p\mathrm{CO_2}$. The overall uncertainty of the $x\mathrm{CO_2}$ measurements and $p\mathrm{CO_2}$ data processing is less than 1 % (Zhai et al., 2005a; Zhai and Dai, 2009).

BGD
10, 7031–7074, 2013

CO_2 concentration in the air near the sea surface was typically determined every 1 to 3 h in the day and every 4 h in the night. The bow intake from which atmospheric air was pumped was installed at 6 to 10 m above the water surface to avoid contamination from the ship. For the purpose of air–sea flux estimation, the air pCO$_2$ data were corrected to 100 % humidity at in situ SST and salinity.

3.4 Sea–air CO_2 flux estimation

The flux calculation was based on the formula $F = k \times K_H \times \Delta p\text{CO}_2$, where k is the gas transfer velocity of CO_2, K_H is the solubility of CO_2 in seawater (Weiss, 1974), and $\Delta p\text{CO}_2$ is the mean sea–air pCO$_2$ difference. A positive flux value represented the net CO_2 exchange from sea to atmosphere and a negative flux value referred to the net CO_2 exchange from atmosphere to sea. Since the k value measured on the spot in the SCS was not available, we used the Sweeney et al. (2007) empirical functions of wind speed at 10 m height (u_{10}) to calculate the value, which is a modification of Wanninkhof (1992). We also calculated the k value based on the latter so that our results would be comparable with those of most other studies.

The Sweeney et al. (2007) (S07 for short) equation is:

$$k\,(\mathrm{cm\,h^{-1}}) = 0.27 \times C2 \times (u_{10}/\mathrm{m\,s^{-1}})^2 \times (Sc/660)^{-0.5} \tag{1}$$

and the Wanninkhof (1992) (W92 for short) equation is:

$$k\,(\mathrm{cm\,h^{-1}}) = 0.31 \times C2 \times (u_{10}/\mathrm{m\,s^{-1}})^2 \times (Sc/660)^{-0.5} \tag{2}$$

where u_{10} is the satellite-derived monthly mean near-surface wind speed; $C2$ is the nonlinearity coefficient, assuming long-term winds followed a Raleigh (Weibull) distribution (Wanninkhof, 1992; Jiang et al., 2008); Sc is the Schmidt number of CO_2 in seawater; and 660 is the Sc value in seawater ($S = 35$) at 20 °C (Wanninkhof, 1992).

Following Wanninkhof (1992) and Jiang et al. (2008), the effect of the short-term variability of wind speeds over a month on the gas transfer velocity was determined

BGD
10, 7031–7074, 2013

using:

$$C2 = \left(u_j^2\right)_{\text{mean}} / (u_{\text{mean}})^2 \quad (3)$$

where u_j is all of the available satellite-derived near surface wind speeds (units: $m\,s^{-1}$, typically twice a day along with the spatial resolution of 25 km) in a month; the subscript "mean" is to calculate the average; and u_{mean} is the monthly mean wind speed (units: $m\,s^{-1}$). The global mean $C2$ has been estimated as 1.27 (Wanninkhof, 2009).

4 Results

4.1 SST and salinity

Generally the seasonal variations of SST in domains A, B, and D followed the seasonal cycle of long-term monthly mean SST at 20° N, 116° E (Fig. 3a). Survey-averaged SST varied between 22.1 ± 1.2 °C in February 2004 in domain A and 30.3 ± 0.4 °C in July 2007 in domain B (Fig. 3a). Domain A was the only area where the lowest survey-averaged SST values of less than 23 °C were observed (Table 3), while we observed the highest SST of 30.82 to 31.65 °C in all domains in July 2007. In domain C, however, the seasonal variation of SST was inconspicuous. Very high SST values between 27.7 ± 1.3 °C in December 2006 and 30.2 ± 0.3 °C in July 2007 were observed in this domain in all seasons (Fig. 3a; Table 5).

Survey-averaged sea surface salinity varied between 32.5 ± 0.6 psu in September 2007 in domain C and 34.3 ± 0.2 psu in February 2006 in domains A and B (Fig. 3b). Most low-salinity values of < 33.5 psu were observed in domains A and C, which were under the influence of river plumes and/or heavy precipitation. In September 2007, the southwestern SCS is highly influenced by the Mekong River Diluted Water (MKRDW) (Chen et al., 2010). Therefore a very low sea surface salinity of 32.5 ± 0.6 psu was observed in domain C (Table 5). Most high-salinity values of > 34.1 psu were detected in domains A and B (Tables 3 and 4).

BGD
10, 7031–7074, 2013

4.2 Wind speed

Survey-averaged wind speed varied between $2.2 \pm 1.5\,m\,s^{-1}$ in February 2006 in domain A and $17.9 \pm 2.1\,m\,s^{-1}$ on 21–22 December 2006 in domain D (Fig. 4a). Most field-survey mean wind speed values were lower than the typical NCEP (National Centers for Environmental Prediction, USA) monthly mean sea surface wind speed (Fig. 4a), presumably due to the ship contamination (Griessbaum et al., 2010) and/or the observation period selected. In contrast, satellite-derived wind speeds showed the same pattern as NCEP data (Fig. 4b). Basically, the sea surface wind was stronger in northeast monsoon seasons than in southwest monsoon seasons. In domain C, the wind was slightly weaker than the other domains (Fig. 4b). Note that we observed a very strong wind with a two-day mean wind speed of $17.9 \pm 2.1\,m\,s^{-1}$ in late December 2006 in domain D (Table 6), which was $\sim 50\,\%$ higher than the typical monthly mean sea surface wind speed (Fig. 4a).

4.3 CO_2 concentrations in the air

Field-measured CO_2 concentrations in the air near the sea surface ranged between 371 ± 3 ppmv in the autumns of 2003/2004 and 393 ± 2 ppmv in April 2008. Over the research period of 6 yr, a reasonable increasing trend was revealed (Fig. 5). In general, both seasonal and inter-annual variations followed the variations of atmospheric CO_2 in the North Pacific Gyre (Mauna Loa station), although terrestrial sources have been found to influence the atmospheric CO_2 over the SCS proper, making atmospheric CO_2 concentrations here more variable than those in the open ocean. It is worth noting that relatively higher atmospheric CO_2 was observed in the northeast monsoon periods and relatively lower atmospheric CO_2 was measured in the southwest monsoon periods.

BGD
10, 7031–7074, 2013

4.4 Distributions of sea surface pCO_2

Figure 2 shows the heterogeneity of sea surface pCO_2 spatial distributions and distinct seasonal cycles in the four domains. In winter, offshore pCO_2 ranged between 286 and 470 µatm (Fig. 2a–c). In general, sea surface pCO_2 increased along with latitude decreasing. This trend was clearly shown during our 1–11 December 2006 survey (Fig. 2c). Typical sea surface pCO_2 in winter could be summarized as 325 to 362 µatm in domain A other than in late December (Table 3), 338 to 385 µatm in domain B (Table 4) and 383 ± 5 µatm in domain C (Table 5). Low pCO_2 of 286 to 300 µatm was measured in February 2004 along the Southern China coastline (Fig. 2a). High pCO_2 of 410 to 470 µatm was measured during the 20–23 December 2006 survey in the area west of the Luzon Strait (Fig. 2c). And extremely high pCO_2 of 1000 to 4500 µatm was detected in the PRE (Fig. 2b; Zhai et al., 2005b). It should be noted that, in domain D we observed a large variation of sea surface pCO_2 between 358 to 379 µatm on 15–16 December 2006 and 379 to 470 µatm on 21–22 December 2006. The peak values of 440 to 470 µatm were observed in the 16 nautical mile sea route around the central site at 18° 42′ N and 119° 35′ E. Similar to the high pCO_2 observed in domain D on 21–22 December 2006, we also measured relatively high pCO_2 of 377 ± 17 µatm in domain A on 22–23 December 2006.

In spring, the sea surface pCO_2 mostly ranged between 340 and 463 µatm (Fig. 2d). pCO_2 also increased along with latitude decreasing. In domain A, sea surface pCO_2 averaged 379 ± 3 µatm in May 2004 and 361 ± 10 µatm in April 2005 (Table 3). In domain B, sea surface pCO_2 averaged 387 ± 15 µatm in both May 2004 and April 2005 (Table 4). In domain C, sea surface pCO_2 averaged 386 ± 7 µatm in May 2004 and 412 ± 14 µatm in April 2005 (Table 5). In domain D, sea surface pCO_2 averaged 370 ± 13 µatm in April 2008 (Table 6). The high pCO_2 values of 400 to 463 µatm were mostly detected in the central/southern basin areas in April 2005. Note that we also observed extremely high pCO_2 values of 700 to 4000 µatm in the PRE and very low pCO_2 values of 234–340 µatm in the Southern Taiwan Strait and in a limited area off the PRE (Fig. 2d).

BGD
10, 7031–7074, 2013

In summer, most offshore pCO_2 values ranged between 350 and 420 µatm, although low values of 280 to 350 µatm were observed in domain A in July 2004 and July 2007 (Fig. 2e and f), and relatively high values of 420 to 440 µatm (Fig. 2f) were associated with a cyclonic cold eddy in the southwestern SCS (Chen et al., 2010; Hu et al., 2011). In domain A, the average was 363 ± 26 µatm in July 2004 and 350 ± 29 µatm in July 2007 (Table 3); in domain B, 383 ± 11 µatm in July 2004 and 404 ± 6 µatm in July 2007 (Table 4); in domain C, 404 ± 6 µatm in July 2007 and 410 ± 14 µatm in August 2007 (Table 5); and in domain D, 400 ± 6 µatm in July 2007 (Table 6). However, in the PRE and at several coastline observation sites, both high pCO_2 values of 440 to 720 µatm and low values of 229 to 280 µatm were observed (Fig. 2e and f; Zhai et al., 2009).

In autumn, offshore pCO_2 values ranged between 340 and 440 µatm, while high pCO_2 values of 440 to 640 µatm were observed along the southwestern coast of the Taiwan Strait. Despite several signals of possible inter-annual and intra-seasonal variation, generally homogeneous pCO_2 distribution was revealed in this transitional season between summer and winter. In domain A, sea surface pCO_2 values averaged 365 ± 14 µatm during most autumn cruises other than in September 2007. During the latter cruise, a relatively high sea surface pCO_2 value of 383 ± 5 µatm was revealed in domain A (Table 3). In domain B, sea surface pCO_2 values ranged from 355 ± 3 µatm in October 2003 through 364 ± 3 µatm in September 2004 to 369 ± 9 µatm in October–November 2006 (Table 4). Relatively high sea surface pCO_2 values of 383 ± 5 µatm were also measured during the September 2007 cruise in domain B. In domain C, sea surface pCO_2 was 367 ± 9 µatm in October 2003 and 402 ± 9 µatm in September 2007 (Table 5). In domain D, sea surface pCO_2 was 361 ± 3 µatm in September 2004 (Table 6).

To summarize, in domain A, relatively low sea surface pCO_2 values of 320 to 390 µatm were observed in all four seasons (Table 3); in domain B, a typical seasonal cycle of relatively high pCO_2 in the warm seasons and relatively low pCO_2 in the cold seasons was revealed (Table 4); in domain C, relatively high sea surface pCO_2 values

BGD
10, 7031–7074, 2013

of 360 to 425 µatm were observed all round a year (Table 5); and in domain D, pCO_2 was particularly dynamic in winter (Fig. 2c; Table 6).

4.5 Air–sea CO_2 flux estimation

Tables 3 to 6 summarize the sea–air CO_2 flux calculations along cruise tracks in the four domains. If we assumed that these cruise track fluxes were representative of the domains, we could obtain an overview of the seasonal variation of CO_2 air–sea exchange in the SCS proper being studied (Fig. 6). In this study, we used satellite-derived monthly averaged wind speeds and the S07 equation (Eq. 1) to calculate gas transfer velocities and then sea–air CO_2 fluxes. We also calculated sea–air CO_2 fluxes based on the W92 equation (Eq. 2) in order to better compare with other studies. The stimulatory effect of short-term variability in wind-speed on the integrated gas transfer (Bates and Merlivat, 2001) was expressed using the nonlinearity coefficient $C2$ (Eq. 3), following Wanninkhof (1992) and Jiang et al. (2008). During our study period, $C2$ varied between 1.04 (high wind/winter) to 1.43 (low wind/spring–summer), and this is very close to the global average of 1.27 (Wanninkhof, 2009), although the variation in range was greater than 1.13 to 1.26 (averaged 1.18) on the US Southeastern shelf (Jiang et al., 2008).

It must be pointed out that the pCO_2 variability in the SCS proper was still remarkable both in terms of time and space. Tables 3 to 6 synthesize the temporal-spatial variability of field-measured data and the estimated sea–air CO_2 fluxes. It should be noted that we reported mostly the temporal variability of CO_2 fluxes based on respective cruises/surveys in a season. If only one cruise was available, however, we reported an error based on standard deviations in wind speeds and/or the aqueous pCO_2. These represent the two largest sources of variations/uncertainties in estimating regional air–sea CO_2 fluxes, i.e. the uncertainty/variation introduced by pCO_2 interpolation and/or extrapolation and the uncertainty introduced by environmental forcing parameters such as wind (Wanninkhof et al., 2009; Johnson et al., 2011).

In domain A, the sea area moderately absorbed CO_2 from the atmosphere in winter ($4.8 \pm 2.6\,\mathrm{mmol\,m^{-2}\,d^{-1}}$), while the air–sea CO_2 exchanges were nearly in equilibrium

BGD
10, 7031–7074, 2013

in spring, summer and autumn (Table 3). In domain B, the air–sea CO_2 exchanges were nearly in equilibrium in winter and autumn, and the sea area only weakly released CO_2 into the atmosphere in spring and summer ($1.7 \pm 0.8\,mmol\,m^{-2}\,d^{-1}$ and $3.2 \pm 0.3\,mmol\,m^{-2}\,d^{-1}$, respectively) (Table 4). In domain C, the sea area released CO_2 into the atmosphere all through the year (Table 5) and the seasonal sea–air CO_2 fluxes ranged from the relatively low value of $1.9 \pm 0.5\,mmol\,m^{-2}\,d^{-1}$ in winter to the very high value of $6.6 \pm 2.4\,mmol\,m^{-2}\,d^{-1}$ in summer. In domain D, the sea–air CO_2 exchanges varied from weak CO_2 uptake in spring ($-1.1 \pm 1.5\,mmol\,m^{-2}\,d^{-1}$) to weak CO_2 release in summer ($2.6 \pm 0.4\,mmol\,m^{-2}\,d^{-1}$), and were nearly in equilibrium with the atmosphere in autumn (Table 6). In winter, domain D varied very much from a typically weak CO_2 sink in early winter to a significant CO_2 source associated with a monsoon driven upwelling event.

Overall, the seasonal pattern of sea–air CO_2 fluxes substantially differed among the four physical-biogeochemical domains under study. Although the annual sea–air CO_2 exchanges were nearly in equilibrium ($-0.44 \pm 0.65\,mol\,m^{-2}\,yr^{-1}$) in domain A, most areas in the SCS proper served as weak sources to the atmospheric CO_2 on an annual basis, with sea–air CO_2 fluxes of $0.46 \pm 0.43\,mol\,m^{-2}\,yr^{-1}$ in domain B; $1.37 \pm 0.55\,mol\,m^{-2}\,yr^{-1}$ in domain C; and $1.21 \pm 1.47\,mol\,m^{-2}\,yr^{-1}$ in domain D (Fig. 6).

5 Discussion

5.1 Factors influencing sea surface pCO_2

In the oligotrophic northern SCS, it has been reported that temperature is the most important factor influencing the seasonal variation of sea surface pCO_2 (Zhai et al., 2005a; Tseng et al., 2007). According to Zhai et al. (2005a), the SST-driven pCO_2 values (in µatm) in the northern SCS vary in the range $(370 \pm 20) \times e^{0.0423(SST-26)}$, where 370 ± 20 is the range of local atmospheric pCO_2 (in µatm), $0.0423\,^{\circ}C^{-1}$ is the coefficient for the temperature effect of sea water pCO_2 (Takahashi et al., 1993), and 26 is the annual average SST (in °C) in the offshore area of the northern SCS (Fig. 3a). In our study, however, we revealed a diverse relationship between pCO_2 and SST in the four different domains of the SCS proper as illustrated in Figs. 7a, 8a, 9a and 10a. To further examine the pCO_2 control mechanism, we also plotted temperature-normalized pCO_2 values (with the coefficient of 4.23 % °C^{-1} to a fixed temperature of 26 °C) against salinity (Figs. 7b, 8b, 9b and 10b).

In domain A, pCO_2 basically increased along with SST, although many pCO_2 values declined to the very low range of 280 to 320 µatm in the two summer cruises (Fig. 7a). Plots of temperature normalized pCO_2 versus salinity (Fig. 7b) revealed that many of those summer data were associated with an estuarine plume (with a salinity of less than 33), where biological productivity was enhanced in the surface water due to nutrient support from the eutrophicated PRE (Cao et al., 2011; Han et al., 2012). The plot of pCO_2 versus SST during 22–23 December 2006 was different from other winter plots in this region (Fig. 7a), and was even different from another dataset obtained during 12–15 December 2006 (Fig. 7a), despite the small interval of only 7 to 10 days between the two surveys. Plots of temperature normalized pCO_2 versus salinity (Fig. 7b) suggested that surface waters during the two December 2006 surveys might have originated from different water sources. Approximately four days before the 22–23 December 2006 survey, a strong northeast monsoon came in. The monsoon might have driven colder and pCO_2-higher coastal waters from the Taiwan Strait into the northeastern part of domain A under survey (Fig. 2c). Similar monsoon-driven nutrient transport from the Taiwan Strait into the northeast SCS shelf was observed by Han et al. (2013).

Excluding the two July datasets and the 22–23 December 2006 dataset, the other 10 surveys showed a linear positive correlation between pCO_2 and SST in domain A (Fig. 7a). In cold seasons the field-measured pCO_2 data were slightly higher than the predicted values based on thermodynamically controlling functions, while in warm seasons relatively lower pCO_2 values were measured (Fig. 7a). Moreover, temperature normalized pCO_2 during these 10 surveys showed a clear seasonal cycle in the water

BGD
10, 7031–7074, 2013

mass with a salinity higher than 33.5 (Fig. 7b). The typical temperature normalized pCO_2 (at 26 °C) ranged between 380 and 420 µatm in the winter cruises, while in the warm seasons most of the temperature normalized pCO_2 (at 26 °C) ranged from 330 to 370 µatm (Fig. 7b). The former (relatively higher than atmospheric equilibrated level) might have resulted from enhanced water mixing between surface water and CO_2-rich subsurface waters in winter. The latter (atmospheric equilibrated level or less) might have originated from CO_2 degassing of the surface water for several months following stratification enhancement in spring.

In domain B, most plots of pCO_2 versus temperature were similar to those in the high salinity areas in domain A, although the field-measured pCO_2 data during April 2005 surveys were slightly higher than those predicted based on thermodynamically controlling lines (Fig. 8a). The SST data measured during the April 2005 surveys were significantly lower than those obtained in May 2004 (26.3 ± 0.9 °C vs. 28.6 ± 0.8 °C, Table 4), suggesting that they might have been influenced by a vertical mixing event in early spring. Figure 7a indeed suggested that many April 2005 data followed the same thermodynamically controlling line as the two February (in winter) datasets. The relationships between temperature normalized pCO_2 and salinity were random in domain B (Fig. 8b).

In domain C, the influences of both SST and salinity on pCO_2 showed no clear trend, although a weakly negative correlation of pCO_2 and SST and a positive correlation of temperature normalized pCO_2 versus salinity were observed in the southwestern SCS on September 2007 (Fig. 9). During the late August and early September surveys in 2007, the influence of MKRDW was coupled with two offshore cold eddies in the southwestern SCS (Chen et al., 2010). According to Chen et al. (2010), the MKRDW was identified with a salinity less than 33.2 and an SST higher than 29.0 °C during the September 2007 survey, while the two cold eddies had a relatively high salinity of > 33.2 and a relatively low SST of ~ 28.2 °C at the center. Figure 9a shows that both the highest pCO_2 value (~ 430 µatm) and the lowest pCO_2 value (~ 380 µatm) during the September 2007 survey were observed in the MKRDW area. In the September eddy (eddy II in Chen et al., 2010), a relatively narrow pCO_2 range of 393 to 423 µatm (Fig. 9a) was observed. In the August eddy (eddy I in Chen et al., 2010) however, a relatively wide pCO_2 range of 383 to 440 µatm (Fig. 9a) was revealed. Figure 9b suggests that the three end-member water mixing occurred in the southwestern SCS in both late summer and early autumn. The low-salinity MKRDW was identified with a relatively low temperature normalized pCO_2 (at 26 °C) of 320 to 340 µatm (Fig. 9b). The high salinity area (with a salinity higher than 33.2) was influenced by two water end-members. One had the similar temperature normalized (at 26 °C) pCO_2 values of 330 to 345 µatm as the MKRDW. Another high salinity water mass was identified with relatively low SST (Chen et al., 2010) but significantly high temperature normalized (at 26 °C) pCO_2 values of 375 to 400 µatm (Fig. 9b), which were influenced by cold eddies, similar to the phenomenon observed in the lee of the main Hawaiian Islands (Chen et al., 2007b). Detailed influences of the two cold eddies on air–sea CO_2 fluxes in the southwestern SCS in late summer and early autumn will be addressed elsewhere.

In domain C, if the influences of the MKRDW and cold eddies were excluded, the seasonal temperature normalized (at 26 °C) pCO_2 varied from 300–330 µatm in October 2003 (autumn), to 345–418 µatm in April 2005 (early spring) and 335–425 µatm in December 2006 (early winter) (Fig. 9b). This seasonal cycle of temperature normalized pCO_2 might also have resulted from enhanced water mixing between surface water and CO_2-rich subsurface waters in winter/early spring and the CO_2 degassing of the surface water for several months following stratification enhancement in spring.

In domain D, a negative relationship between pCO_2 and SST was observed during the 21–22 December 2006 survey (Fig. 10a). Two days before our survey, Xu et al. (2009) observed a similar phenomenon in the sea surface on the adjacent coast. Based on multiple comparisons of temperature, salinity and nutrient concentrations, they conclude that the low-temperature (∼ 24 °C) water with a high-pCO_2 (∼ 460 µatm) level is upwelled from the 45 to 80 m depth (Xu et al., 2009). Actually, the strong northeast monsoon came in three days before the 21–22 December 2006 survey. Even when the monsoon had weakened, a strong northeast wind

BGD
10, 7031–7074, 2013

($17.9 \pm 2.1\,m\,s^{-1}$ during our two-day survey versus $9.8 \pm 2.0\,m\,s^{-1}$ before the event) was observed (Fig. 4a). Based on satellite-derived SST images (Tropical Rainfall Measuring Mission/Microwave Imager) on 22–23 December 2006, a relatively cold (~ 22 °C vs. the neighboring 25.0 ± 0.9 °C) area was revealed between 18° 30′ and 20° 00′ N and 118° 30′ and 120° 30′ E (C. Y. Zhang, unpublished data), indicating that upwelling might occur, which resulted in the negative relationship between $p\mathrm{CO_2}$ and SST, and thus a significant CO_2 degassing event. The CO_2 effects of this monsoon driven offshore upwelling were comparable to the nearby coastal upwelling reported by Xu et al. (2009). Peak levels of the offshore high $p\mathrm{CO_2}$ were revealed to be 460–470 µatm (Xu et al., 2009) and in this study (Fig. 10a). Since the strong northeast monsoon drove the climatologically cold eddy in the west Luzon Strait in winter, i.e. the Luzon Gyre, the wintertime CO_2 degassing events might have contributed to the seasonal characteristics of air–sea CO_2 exchange in this region. However, this winter air–sea CO_2 exchange was subject to huge variability due to rapid CO_2 degassing and upwelled nutrients driven primary production in the surface waters. In January 2010, Shang et al. (2012) note intensive phytoplankton blooms in the Luzon Strait and its vicinity. The associated sea surface $p\mathrm{CO_2}$ at this time was 10 to 20 µatm lower than the atmospheric equilibrated level (M. Dai et al., unpublished data).

In summary, besides the general pattern of temperate controlled seasonal variation of sea surface $p\mathrm{CO_2}$ in the SCS, the influences of river plume with low $p\mathrm{CO_2}$, water mixing between surface water and CO_2-rich subsurface waters in cold seasons, CO_2 degassing from the surface water in warm seasons, and episodic events of eddy and upwelling around the SCS also impose high variability on surface $p\mathrm{CO_2}$ distribution, as well as air–sea CO_2 flux estimation.

BGD
10, 7031–7074, 2013

5.2 Impact of winter monsoon induced events of CO_2 degassing on the annual air–sea CO_2 fluxes

Most of above-discussed datasets reflected climatological variations in the respective domains. It must be pointed out, however, that many episodic events might significantly impact on the CO_2 fluxes. An example is the winter monsoon induced CO_2 degassing event observed in domain D in late December 2006 described above. As shown in Table 6, the area averaged sea–air CO_2 fluxes increased by $\sim 27\,\mathrm{mmol\,m^{-2}\,d^{-1}}$ within a time lag of one week, due to upwelling of the subsurface water. This change was much greater than a similar phenomenon in spring in the lee of the main Hawaiian Islands (Chen et al., 2007b) but was similar to that observed in equatorial upwelling areas in the eastern Pacific (Chavez et al., 1999). To further evaluate the amount of CO_2 released during this event, we assumed that the Revelle factor (RF) of the upwelled water was ~ 10, the $\mathrm{DIC_{avg}} \sim 2000\,\mathrm{\mu mol\,L^{-1}}$, the aqueous $p\mathrm{CO_{2,avg}} \sim 410\,\mathrm{\mu atm}$, and the air-saturated $p\mathrm{CO_2} \sim 375\,\mathrm{\mu atm}$. Based on the eloquent definition of RF given by Sundquist et al. (1979), the oversaturated and then releasable DIC could therefore be estimated via $\Delta\mathrm{DIC} = \Delta p\mathrm{CO_2}/p\mathrm{CO_{2,avg}}/\mathrm{RF} \times \mathrm{DIC_{avg}}=(410-375)/410/10 \times 2000=17\,\mathrm{\mu mol\,L^{-1}}$. Given that the upper mixed layer depth was 45–80 m (Xu et al., 2009), the eddy-related CO_2 release should be 0.76 to 1.36 $\mathrm{mol\,m^{-2}}$. This was comparable with the typical annual CO_2 release in domain D (Fig. 6).

This case showed that the very strong winter monsoon not only caused a high gas transfer velocity, but also enhanced vertical water mixing. When the CO_2-rich subsurface water is mixed with the surface water, a winter CO_2 sink area in the subtropical ocean might be reversed into a winter source area. Due to surveying difficulties, very few cases of winter CO_2 source events are found in the winter CO_2 sink database. In such a case, if we neglected the CO_2 variability due to monsoon-induced eddies, the annually based air–sea CO_2 flux would be nearly zero (Table 6). Thus, the winter monsoon induced CO_2 degassing events had substantial impacts on the annually

BGD
10, 7031–7074, 2013

based air–sea CO_2 fluxes. This issue clearly needs further investigation despite the difficulties in observation.

6 Concluding remarks

This study clearly showed that neither snap-shot based nor time series station based investigations were sufficient to adequately assess air–sea CO_2 fluxes in an ocean margin which is often characterized by tremendous dynamic environments. In the largest tropical marginal sea, the SCS, this research was the first attempt to simultaneously resolve coverage in both time and space. We analyzed the temporal-spatial variations and the controlling mechanisms of sea surface pCO_2 in the SCS proper. We also estimated the air–sea CO_2 fluxes and their temporal-spatial variability based on 14 mapping cruises. Although the pCO_2 variability in the SCS proper was remarkable both in time and space, and the critical roles of wind speed variability and the gas transfer velocity in the annual air–sea CO_2 flux estimation are still unresolved, this study demonstrated once more that the SCS as a whole serves as a weak source of atmospheric CO_2 (Zhai et al., 2005a; Chen et al., 2006; Dai et al., 2013). In shaping this source term at least in the basin area of the SCS, the inflow of the CO_2-enriched North Pacific deep water through the Luzon Strait and its subsequent upward transport into the thermocline through vertical mixing and upwelling may have played a critically important role (Dai et al., 2013).

Taken together the four physical-biogeochemical domains under study, it released $18 \pm 10\,\mathrm{Tg\,C\,yr^{-1}}$ ($\mathrm{Tg} = 10^{12}\,\mathrm{g}$). If we extrapolated such an average flux to the whole SCS, we would derive a flux value of $47\,\mathrm{Tg\,C\,yr^{-1}}$, and thus, the SCS, which represents 4 % of the surface area of the global tropical oceans, accounts for 6.8 % of CO_2 emission, as compared with the overall CO_2 emission rate of the global oceanic equatorial belt of $690\,\mathrm{Tg\,C\,yr^{-1}}$ (Takahashi et al., 2009). Even considering the fact that the CO_2 uptakes of the Amazon River plume (Ternon et al., 2000; Körtzinger, 2003; Cooley and Yager, 2006; Cooley et al., 2007) counteract the CO_2 source of the global tropical oceans, the CO_2 release rate of the SCS might exceed the average CO_2 emission level of most tropical oceans.

Acknowledgements. We thank Yi Wang, Gui Chen, Zhaozhang Chen, Ke Liu, Benwang Wang and Zhimian Cao for assistance in the data collection during several cruises, and Professor John Hodgkiss for his assistance with English. Jiwei Tian, Pinghe Cai and the crews of R/V *Shiyan 3*, R/V *Dongfanghong 2*, R/V *Yanping 2*, R/V *Kexue 3* and R/V *Haijian 83* provided much help during the sampling cruises. The research was jointly supported by the National Basic Research Program of China (2009CB421201), the National Natural Science Foundation of China (NSFC) (41130857, 41121091, 41206061, 41076044 and 90711005), and the State Oceanic Administration of China (contract DOMEP-MEA-01-10). Sampling surveys were supported by the NSFC (90211020, 40490264 and 40521003), and the South China Sea Institute of Oceanology (SCSIO, CAS, China) via the Integrated Nansha Scientific Investigation Cruise 2004 and the Northern South China Sea Open Cruise 2004; the National High-Tech Research and Development Program ("863" Program) of China (via the project of Quality Control/in situ Standardization Experiment 2007); and the China Sea Open Cruise 2006 using R/V *Kexue 3* (Institute of Oceanology, CAS, China).

References

Bates, N. R. and Merlivat, L.: The influence of short-term wind variability on air–sea CO_2 exchange, Geophys. Res. Lett., 28, 3281–3284, 2001.

Borges, A. V., Delille, B., and Frankignoulle, M.: Budgeting sinks and sources of CO_2 in the coastal ocean: diversity of ecosystems counts, Geophys. Res. Lett., 32, L14601, doi:10.1029/2005GL023053, 2005.

Borges, A. V.: Present day carbon dioxide fluxes in the coastal ocean and possible feedbacks under global change, in: Oceans and the Atmospheric Carbon Content, edited by: Duart, P. and Santana-Casiano, J. M., Springer, Berlin, 47–77, 2011.

Cai, W.-J.: Estuarine and coastal ocean carbon paradox: CO_2 sinks or sites of terrestrial carbon incineration?, Annu. Rev. Mar. Sci., 3, 123–145, 2011.

Cai, W.-J., Dai, M.-H., and Wang, Y.-C.: Air-sea exchange of carbon dioxide in ocean margins: a province-based synthesis, Geophys. Res. Lett., 33, L12603, doi:10.1029/2006GL026219, 2006.

Cao, Z.-M., Dai, M.-H., Zheng, N., Wang, D.-L., Li, Q., Zhai, W.-D., Meng, F.-F., and Gan, J.-P.: Dynamics of the carbonate system in a large continental shelf system under the influence of both a river plume and coastal upwelling, J. Geophys. Res., 116, G02010, doi:10.1029/2010JG001596, 2011.

Chen, C.-T. A. and Borges, A. V.: Reconciling opposing views on carbon cycling in the coastal ocean: continental shelves as sinks and near-shore ecosystems as sources of atmospheric CO_2, Deep-Sea Res. Part II, 56, 578–590, 2009.

Chen, C.-T. A., Wang, S.-L., Wang, B.-J., and Pai, S.-C.: Nutrient budgets for the South China Sea basin, Mar. Chem., 75, 281–300, 2001.

Chen, C.-T. A., Wang, S.-L., Chou, W.-C., and Sheu, D.-D.: Carbonate chemistry and projected future changes in pH and $CaCO_3$ saturation state of the South China Sea, Mar. Chem., 101, 277–305, 2006.

Chen, F.-Z., Cai, W.-J., Benitez-Nelson, C., and Wang, Y.-C.: Sea surface pCO$_2$–SST relationships across a cold-core cyclonic eddy: implications for understanding regional variability and air–sea gas exchange, Geophys. Res. Lett., 34, L10603, doi:10.1029/2006GL028058, 2007b.

Chen, W.-F., Liu, Q., Huh, C.-A., Dai, M.-H., and Miao, Y.-C.: Signature of the Mekong River plume in the western South China Sea revealed by radium isotopes, J. Geophys. Res., 115, C12002, doi:10.1029/2010JC006460, 2010.

Chen, Y.-L. L. and Chen, H.-Y.: Seasonal dynamics of primary and new production in the northern South China Sea: the significance of river discharge and nutrient advection, Deep-Sea Res. Part I, 53, 971–986, 2006.

Chen, Y.-L. L., Chen, H.-Y., Lin, I.-I., Lee, M.-A., and Chang, J.: Effects of cold eddy on phytoplankton production and assemblages in Luzon Strait bordering the South China Sea, J. Oceanogr., 63, 671–683, 2007a.

Chou, W.-C., Sheu, D.-D., Chen, C.-T. A., Wang, S.-L., and Tseng, C.-M.: Seasonal variability of carbon chemistry at the SEATS time-series site, northern South China Sea between 2002 and 2003, Terr. Atmos. Ocean. Sci., 16, 445–465, 2005.

Chavez, F. P., Strutton, P. G., Friederich, G. E., Feely, R. A., Feldman, G. C., Foley, D. G., and McPhaden, M. J.: Biological and chemical response of the equatorial Pacific Ocean to the 1997–98 El Niño, Science, 286, 2126–2131, 1999.

BGD
10, 7031–7074, 2013

Cooley, S. R. and Yager, P. L.: Physical and biological contributions to the western tropical North Atlantic Ocean carbon sink formed by the Amazon River plume, J. Geophys. Res., 111, C08018, doi:10.1029/2005JC002954, 2006.

Cooley, S. R., Coles, V. J., Subramaniam, A., and Yager, P. L.: Seasonal variations in the Amazon plume-related atmospheric carbon sink, Global Biogeochem. Cy., 21, GB3014, doi:10.1029/2006GB002831, 2007.

Dai, M.-H., Zhai, W.-D., Cai, W.-J., Callahan, J., Huang, B.-Q., Shang, S.-L., Huang, T., Li, X.-L., Lu, Z.-M., Chen, W.-F., and Chen, Z.-Z.: Effects of an estuarine plume-associated bloom on the carbonate system in the lower reaches of the Pearl River estuary and the coastal zone of the northern South China Sea, Cont. Shelf Res., 28, 1416–1423, 2008.

Dai, M.-H., Lu, Z.-M., Zhai, W.-D., Chen, B.-S., Cao, Z.-M., Zhou, K.-B., Cai, W.-J., and Chen, C.-T. A.: Diurnal variations of surface seawater $p\mathrm{CO_2}$ in contrasting coastal environments, Limnol. Oceanogr., 54, 735–745, 2009.

Dai, M.-H., Cao, Z.-M., Guo, X.-H., Zhai, W.-D., Liu, Z.-Y., Yin, Z.-Q., Xu, Y.-P., Gan, J.-P., Hu, J.-Y., and Du, C.-J.: Why are some marginal seas sources of atmospheric CO_2?, Geophys. Res. Lett., 40, in press, doi:10.1002/grl.50390, 2013.

Gan, J.-P., Li, L., Wang, D.-X., and Guo, X.-G.: Interaction of a river plume with coastal upwelling in the northeastern South China Sea, Cont. Shelf Res., 29, 728–740, 2009.

Griessbaum, F., Moat, B. I., Narita, Y., Yelland, M. J., Klemm, O., and Uematsu, M.: Uncertainties in wind speed dependent CO_2 transfer velocities due to airflow distortion at anemometer sites on ships, Atmos. Chem. Phys., 10, 5123–5133, doi:10.5194/acp-10-5123-2010, 2010.

Han, A.-Q., Dai, M.-H., Kao, S.-J., Gan, J.-P., Li, Q., Wang, L.-F., Zhai, W.-D., and Wang, L.: Nutrient dynamics and biological consumption in a large continental shelf system under the influence of both a river plume and coastal upwelling, Limnol. Oceanogr., 57, 486–502, 2012.

Han, A., Dai, M., Gan, J., Kao, S.-J., Zhao, X., Jan, S., Li, Q., Lin, H., Chen, C.-T. A., Wang, L., Hu, J., Wang, L., and Gong, F.: Inter-shelf nutrient transport from the East China Sea as a major nutrient source supporting winter primary production on the northeast South China Sea shelf, Biogeosciences Discuss., 10, 3891–3923, doi:10.5194/bgd-10-3891-2013, 2013.

Han, W.-Y.: Marine Chemistry in the South China Sea, Science Press, Beijing, 289 pp., 1998 (in Chinese).

Hu, J.-Y., Gan, J.-P., Sun, Z.-Y., Zhu, J., and Dai, M.-H.: Observed three-dimensional structure of a cold eddy in the southwestern South China Sea, J. Geophys. Res., 116, C05016, doi:10.1029/2010JC006810, 2011.

BGD
10, 7031–7074, 2013

Seasonal variations of air-sea CO_2 fluxes in the South China Sea

W.-D. Zhai et al.

Jiang, L.-Q., Cai, W.-J., Wanninkhof, R., Wang, Y., and Lüger, H.: Air–sea CO_2 fluxes on the US South Atlantic Bight: spatial and seasonal variability, J. Geophys. Res., 113, C07019, doi:10.1029/2007JC004366, 2008.

Jo, Y.-H., Dai, M.-H., Zhai, W.-D., Yan, X.-H., and Shang, S.-L.: On the variations of sea surface pCO_2 in the northern South China Sea: a remote sensing based neural network approach, J. Geophys. Res., 117, C08022, doi:10.1029/2011JC007745, 2012.

Johnson, M. T., Hughes, C., Bell, T. G., and Liss, P. S.: A Rumsfeldian analysis of uncertainty in air–sea gas exchange, in: Gas Transfer at Water Surfaces, Kyoto University Press, 464–485, 2011.

Körtzinger, A.: A significant CO_2 sink in the tropical Atlantic Ocean associated with the Amazon River plume, Geophys. Res. Lett., 30, 2287, doi:10.1029/2003GL018841, 2003.

Laruelle, G. G., Dürr, H. H., Slomp, C. P. and Borges, A. V.: Evaluation of sinks and sources of CO_2 in the global coastal ocean using a spatially explicit typology of estuaries and continental shelves, Geophys. Res. Lett., 37, L15607, doi:10.1029/2010GL043691, 2010.

Li, L., Nowlin, W. and Su, J.-L.: Anticyclonic rings from the Kuroshio in the South China Sea, Deep-Sea Res. Part I, 45, 1469–1482, 1998.

Liu, K.-K., Atkinson, L., Quiñones, R. A., and Talaue-McManus, L.: Biogeochemistry of continental margins in a global context, in: Carbon and Nutrient Fluxes in Continental Margins – a Global Synthesis, edited by: Liu, K.-K., Atkinson, L., Quiñones, R., and Talaue-McManus, L., Springer, Berlin, 3–24, 2010.

Ning, X.-R., Chai, F., Xue, H.-J., Cai, Y., Liu, C., and Shi J.: Physical-biological oceanographic coupling influencing phytoplankton and primary production in the South China Sea, J. Geophys. Res., 109, C10005, doi:10.1029/2004JC002365, 2004.

Rehder, G. and Suess, E.: Methane and pCO_2 in the Kuroshio and the South China Sea during maximum summer surface temperatures, Mar. Chem., 75, 89–109, 2001.

Sasai, Y., Sasaki, H., and Richards, K. J.: Impact of physical processes on the phytoplankton blooms in the South China Sea: an eddy-resolving physical-biological model study, Biogeosciences Discuss., 10, 1577–1604, doi:10.5194/bgd-10-1577-2013, 2013.

Shang, S.-L., Li, L., Li J., Li, Y.-H., Lin, G., and Sun, J.: Phytoplankton bloom during the northeast monsoon in the Luzon Strait bordering the Kuroshio, Remote Sens. Environ., 124, 38–48, 2012.

Sheu, D.-D., Chou, W.-C., Wei, C.-L., Hou, W.-P., Wong, G. T. F., and Hsu, C.-W.: Influence of El Niño on the sea-to-air CO_2 flux at the SEATS time-series site, northern South China Sea, J. Geophys. Res., 115, C10021, doi:10.1029/2009JC006013, 2010b.

Sheu, W.-J., Wu, C.-R., and Oey, L.-Y.: Blocking and westward passage of eddies in the Luzon Strait, Deep-Sea Res. Part II, 57, 1783–1791, 2010a.

Smith, S. V. and Hollibaugh, J. T.: Coastal metabolism and the oceanic organic carbon balance, Rev. Geophys., 31, 75–89, 1993.

Sundquist, E. T., Plummer, L. N., and Wigley, T. M. L.: Carbon dioxide in the ocean surface: the homogenous buffer factor, Science, 204, 1203–1205, 1979.

Sweeney, C., Gloor, E., Jacobson, A. R., Key, R. M., McKinley, G., Sarmiento, J. L., and Wanninkhof, R.: Constraining global air–sea gas exchange for CO_2 with recent bomb ^{14}C measurements, Global Biogeochem. Cy., 21, GB2015, doi:10.1029/2006GB002784, 2007.

Takahashi, T., Olafsson, J., Goddard, J. G., Chipman, D. W., and Sutherland, S. C.: Seasonal variation of CO_2 and nutrients in the high-latitude surface oceans: a comparative study, Global Biogeochem. Cy., 7, 843–878, 1993.

Takahashi, T., Sutherland, S. C., Wanninkhof, R., Sweeney, C., Feely, R. A., Chipman, D. W., Hales, B., Friederich, G., Chavez, F., Sabine, C., Watson, A., Bakker, D. C. E., Schuster, U., Metzl, N., Yoshikawa-Inoue, H., Ishii, M., Midorikawa, T., Nojiri, Y., Kortzinger, A., Steinhoff, T., Hoppema, M., Olafsson, J., Arnarson, T. S., Tilbrook, B., Johannessen, T., Olsen, A., Bellerby, R., Wong, C. S., Delille, B., Bates, N. R., and de Baar, H. J. W.: Climatological mean and decadal change in surface ocean pCO_2, and net sea–air CO_2 flux over the global oceans, Deep-Sea Res. Part II, 56, 554–577, 2009.

Tan, S.-C. and Shi G.-Y.: Spatiotemporal variability of satellite-derived primary production in the South China Sea, 1998–2006, J. Geophys. Res., 114, G03015, doi:10.1029/2008JG000854, 2009.

Ternon, J. F., Oudot, C., Dessier, A., and Diverres, D.: A seasonal tropical sink for atmospheric CO_2 in the Atlantic Ocean: the role of the Amazon River discharge, Mar. Chem., 68, 183–201, 2000.

Tseng, C.-M., Wong, G. T. F., Chou, W.-C., Lee, B.-S., Sheu, D.-D., and Liu, K.-K.: Temporal variations in the carbonate system in the upper layer at the SEATS station, Deep-Sea Res. Part II, 54, 1448–1468, 2007.

Tsunogai, S., Watanabe, S., and Sato, T.: Is there a “continental shelf pump” for the absorption of atmospheric CO_2?, Tellus B, 51, 701–712, 1999.

Xu, Y.-P., Dai, M.-H., Zhai, W.-D., Yuan, D.-X., Liu, J.-W., Sun, Z.-Y., Lin, H., and Wu, J.-Y.: Short-term dynamics of nutrients influenced by upwelling in a small oligotrophic coastal ecosystem, Gan Bay, in the northwest Philippines, Prog. Nat. Sci., 19, 595–601, 2009.

Walsh, J. J., Rowe, G. T., Iverson, R. L., and McRoy, C. P.: Biological export of shelf carbon is a sink of the global CO_2 cycle, Nature, 291, 196–201, 1981.

Wanninkhof, R.: Relationship between wind-speed and gas-exchange over the ocean, J. Geophys. Res., 97, 7373–7382, 1992.

Wanninkhof, R., Asher, W. E., Ho, D. T., Sweeney, C., and McGillis, W. R.: Advances in quantifying air–sea gas exchange and environmental forcing, Annu. Rev. Mar. Sci., 1, 213–244, 2009.

Weiss, R. F.: Carbon dioxide in water and seawater: the solubility of a non-ideal gas, Mar. Chem., 2, 203–215, 1974.

Weiss, R. F. and Price, R. A.: Nitrous oxide solubility in water and seawater, Mar. Chem., 8, 347–359, 1980.

Wong, G. T. F., Ku, T.-L., Mulholland, M., Tseng, C.-M., and Wang, D.-P.: The SouthEast Asian Time-series Study (SEATS) and the biogeochemistry of the South China Sea: an overview, Deep-Sea Res. Part II, 54, 1434–1447, 2007.

Yan, H.-Q., Yu, K.-F., Shi, Q., Tan, Y.-H., Zhang, H.-L., Zhao, M.-X., Li, S., Chen, T.-R., Huang, L.-Y., and Wang, P.-X.: Coral reef ecosystems in the South China Sea as a source of atmospheric CO_2 in summer, Chin. Sci. Bull., 56, 676–684, 2011.

Yuan, Y.-L., Zheng, Q.-A., Dai, D.-J., Hu, X.-M., Qiao, F.-L., and Meng, J.-M.: Mechanism of internal waves in the Luzon Strait, J. Geophys. Res., 111, C11S17, doi:10.1029/2005JC003198, 2006.

Zhai, W. D. and Dai, M. H.: On the seasonal variation of air–sea CO_2 fluxes in the outer Changjiang (Yangtze River) Estuary, East China Sea, Mar. Chem., 117, 2–10, 2009.

Zhai, W.-D., Dai, M.-H., Cai, W.-J., Wang, Y.-C., and Hong, H. S.: The partial pressure of carbon dioxide and air–sea fluxes in the northern South China Sea in spring, summer and autumn, Mar. Chem., 96, 87–97, 2005a. [Erratum: Mar. Chem., 103, 209, 2007].

Zhai, W.-D., Dai, M.-H., Cai, W.-J., Wang, Y.-C., and Wang, Z.-H.: High partial pressure of CO_2 and its maintaining mechanism in a subtropical estuary: the Pearl River estuary, China, Mar. Chem., 93, 21–32, 2005b.

BGD

10, 7031–7074, 2013

Seasonal variations of air-sea CO_2 fluxes in the South China Sea

W.-D. Zhai et al.

Zhai, W. D., Dai, M., and Cai, W.-J.: Coupling of surface pCO_2 and dissolved oxygen in the northern South China Sea: impacts of contrasting coastal processes, Biogeosciences, 6, 2589–2598, doi:10.5194/bg-6-2589-2009, 2009.

BGD
10, 7031–7074, 2013

Table 1. Physical-biogeochemical domains in the South China Sea categorized in the present study.

Domain #	Domain name/ description	Characteristics	Latitude (° N)	Longitude (° E)	Area (10^3 km^2)	Surveying months
A	Off the Pearl River Estuary	Summer river plume, winter cooling	21–23	112–118	68	Oct 2003, Feb 2004, May 2004, Jul 2004, Sep 2004, Apr 2005, Feb 2006, Oct 2006, Nov 2006, Dec 2006, Jul 2007, Sep 2007
B	Northern basin (including the northern slope area)	Oligotrophic, winter cooling	18–21	112–118	209	Oct 2003, Feb 2004, May 2004, Jul 2004, Sep 2004, Apr 2005, Feb 2006, Oct 2006, Nov 2006, Dec 2006, Jul 2007, Sep 2007
C	Central and southern basin	Oligotrophic, warm all the year round, coral reefs	7–18	110–117	928	Oct 2003, May 2004, Apr 2005, Dec 2006, Jul 2007, Aug 2007, Sep 2007
D	West of the Luzon Strait	Oligotrophic, cold eddy in winter	18–22	118–121	139	Sep 2004, Apr 2005, Dec 2006, Jul 2007, Apr 2008

Table 2. Summary of the information of the sampling cruises between 2003 and 2008.

Surveying time	Domain coverage	Seasonal coverage	Sampling depth and RV	Sampler configuration	Refs.
Oct 2003	A, B, C	Autumn	5 m (Shiyan 3)	Modified from Zhai et al. (2005b)	This study
Feb 2004	A, B	Winter	2 m (Yanping 2)	Modified from Zhai et al. (2005b)	This study*
May 2004	B, C	Spring	5 m (Shiyan 3)	Modified from Zhai et al. (2005b)	This study
Jul 2004	A, B	Summer	2 m (Yanping 2)	Modified from Zhai et al. (2005b)	Zhai et al. (2009)
Sep 2004	A, B, D	Autumn	1 m (Shiyan 3)	Modified from Zhai et al. (2005b)	This study
Apr 2005	B, C, D	Spring	5 m (Dongfanghong 2)	Modified from Zhai et al. (2005b)	This study
Feb 2006	A, B	Winter	5 m (Haijian 83)	Modified from Zhai et al. (2005b)	This study
Oct 2006	A, B	Autumn	3 m (Kexue 3)	Modified from Jiang et al. (2008)	This study
Nov 2006	A, B	Autumn	5 m (Dongfanghong 2)	Modified from Jiang et al. (2008)	This study
Dec 2006	A, B, C, D	Winter	5 m (Dongfanghong 2)	Modified from Jiang et al. (2008)	This study
Jul 2007	A, B, D	Summer	5 m (Dongfanghong 2)	Modified from Jiang et al. (2008)	This study
Aug 2007	C	Summer	5 m (Dongfanghong 2)	Modified from Jiang et al. (2008)	This study
Sep 2007	A, B, C	Autumn	5 m (Dongfanghong 2)	Modified from Jiang et al. (2008)	This study
Apr 2008	D	Spring	5 m (Dongfanghong 2)	GO8050, Zhai and Dai (2009)	This study

* Some of the data collected from this cruise in February 2004 has been reported in Jo et al. (2012).

BGD
10, 7031–7074, 2013

Seasonal variations of air-sea CO_2 fluxes in the South China Sea

W.-D. Zhai et al.

Table 3. Summary of pCO_2, salinity and SST along cruise tracks, monthly satellite-derived wind speed, and sea–air CO_2 flux estimation in domain A. *C2* is the nonlinearity effect of the short-term variability of wind speeds over a month on the gas transfer velocity, assuming long-term winds followed a Raleigh (Weibull) distribution (Wanninkhof, 1992; Jiang et al., 2008). See texts for details. Errors in sea–air CO_2 flux estimation are the temporal variability of CO_2 fluxes based on respective cruises/surveys.

Observation time	Aqueous pCO_2 µatm	Air pCO_2 µatm	Salinity psu	SST °C	Wind speed $m\,s^{-1}$	*C2*	Sea–air CO_2 fluxes ($mmol\,CO_2\,m^{-2}\,d^{-1}$) Survey average (W92)	Survey average (S07)	Seasonal average
Feb 2004	334 ± 9 (315–356)	368.7 ± 3.8 (363.5–375.2)	34.28 ± 0.13 (33.97–34.52)	22.1 ± 1.2 (20.45–24.62)	9.3 ± 0.6 (7.9–10.1)	1.18	−8.59	−7.48	
Feb 2006	355 ± 4 (347–365)	370.5 ± 0.3 (370.0–371.1)	34.29 ± 0.18 (33.69–34.75)	23.4 ± 0.4 (22.65–24.05)	10.0 ± 0.4 (8.9–10.7)	1.13	−4.16	−3.63	
12–15 Dec 2006	358 ± 4 (350–371)	No data (375[a])	33.97 ± 0.09 (33.80–34.18)	25.0 ± 0.7 (22.90–25.72)	12.0 ± 0.5 (10.4–12.5)	1.04	−6.29	−5.48	−4.8 ± 2.6 (winter)
22–23 Dec 2006	377 ± 17 (345–415)	381.7 ± 1.8 (378.3–385.1)	34.28 ± 0.18 (33.63–34.51)	22.6 ± 2.1 (19.42–25.36)	12.0 ± 0.5 (10.4–12.5)	1.04	−1.55	−1.35	
May 2004	379 ± 3 (374–384)	359.8 ± 1.4 (358.8–360.8)	34.18 ± 0.06 (34.07–34.29)	28.0 ± 0.3 (27.49–28.41)	5.2 ± 0.3 (4.6–5.6)	1.43	1.80	1.57	
Apr 2005	361 ± 10 (339–378)	371.0 ± 0.1 (370.9–371.1)	34.12 ± 0.17 (33.98–34.52)	25.5 ± 0.9 (23.57–26.48)	5.0 ± 0.3 (4.5–5.5)	1.43	−0.85	−0.74	0.4 ± 1.6 (spring)
Jul 2004	363 ± 26 (312–400)	361.8 ± 8.0 (356.5–373.4)	33.51 ± 0.80 (31.56–34.33)	29.4 ± 0.9 (28.01–30.92)	7.4 ± 0.3 (6.8–8.2)	1.33	0.17	0.15	
Jul 2007	350 ± 29 (281–414)	367.0 ± 1.5 (363.7–370.2)	32.96 ± 0.68 (31.89–34.40)	30.2 ± 0.6 (25.95–31.21)	5.2 ± 0.4 (4.5–5.8)	1.27	−1.49	−1.30	−0.6 ± 1.1 (summer)
Oct 2003	365 ± 14 (349–406)	No data (355[b])	34.20 ± 0.30 (33.43–34.54)	27.8 ± 0.1 (27.59–27.94)	9.5 ± 0.5 (8.2–10.1)	1.12	2.49	2.17	
Sep 2004	360 ± 5 (350–364)	358.3 ± 1.4 (356.0–359.8)	33.52 ± 0.80 (33.02–33.80)	29.1 ± 0.5 (28.62–29.90)	6.2 ± 0.7 (4.7–7.3)	1.39	0.19	0.17	
Oct 2006	360 ± 8 (347–374)	363.3 ± 0.6 (362.1–364.1)	33.67 ± 0.29 (33.02–33.92)	27.4 ± 0.6 (26.71–28.41)	8.4 ± 0.6 (6.8–9.0)	1.14	−0.63	−0.55	0.2 ± 1.9 (autumn)
Nov 2006	361 ± 6 (349–375)	369.4 ± 1.5 (367.6–372.9)	33.87 ± 0.12 (33.57–34.15)	25.9 ± 0.4 (25.14–26.59)	8.9 ± 0.3 (8.2–9.6)	1.22	−1.98	−1.72	
Sep 2007	383 ± 5 (369–396)	366.7 ± 1.7 (364.5–369.6)	33.21 ± 0.15 (32.91–33.42)	28.5 ± 0.9 (27.01–29.31)	7.5 ± 0.4 (6.9–8.4)	1.34	3.02	2.63	

[a] The average of field-measured values between November 2006 and 22–23 December 2006.

[b] The average of field-measured values in domain B in the same cruise (Table 4).

BGD
10, 7031–7074, 2013

Seasonal variations of air-sea CO_2 fluxes in the South China Sea

W.-D. Zhai et al.

Table 4. Summary of pCO_2, salinity and SST along cruise tracks, monthly satellite-derived wind speed, and sea–air CO_2 flux estimation in domain B. *C*2 and the errors in sea–air CO_2 flux estimation are the same as in Table 3. See texts for details.

Observation time	Aqueous pCO_2 µatm	Air pCO_2 µatm	Salinity psu	SST °C	Wind speed $m\,s^{-1}$	*C*2	Sea–air CO_2 fluxes ($mmol\,CO_2\,m^{-2}\,d^{-1}$)		
							Survey average (W92)	Survey average (S07)	Seasonal average
Feb 2004	344 ± 6 (324–362)	365.6 ± 2.7 (361.4–371.1)	34.19 ± 0.12 (33.81–34.38)	23.0 ± 0.7 (21.90–24.70)	7.8 ± 0.9 (6.5–10.1)	1.19	−3.86	−3.36	
Feb 2006	367 ± 11 (342–398)	372.6 ± 2.8 (368.9–377.7)	34.29 ± 0.19 (33.78–34.75)	23.8 ± 0.7 (22.50–25.29)	8.9 ± 0.7 (7.4–10.2)	1.14	−1.28	−1.12	−0.9 ± 1.9 (winter)
11–12 Dec 2006	376 ± 9 (357.2–393.0)	No data (375*)	33.86 ± 0.12 (33.73–34.14)	25.9 ± 0.7 (24.33–26.49)	11.9 ± 0.5 (9.7–12.9)	1.04	0.53	0.46	
May 2004	386 ± 9 (369-398)	356.9 ± 1.7 (355.5–359.4)	34.16 ± 0.15 (33.90–34.38)	28.6 ± 0.8 (26.98–29.57)	4.9 ± 0.4 (4.1–6.1)	1.49	2.57	2.24	1.7 ± 0.8 (spring)
Apr 2005	387 ± 15 (363–444)	373.0 ± 2.6 (367.7–376.1)	34.08 ± 0.10 (33.86–34.25)	26.3 ± 0.9 (24.45–27.92)	5.2 ± 0.6 (4.1–6.5)	1.33	1.26	1.09	
Jul 2004	383 ± 11 (353–417)	357.7 ± 1.1 (355.7–360.4)	34.17 ± 0.17 (33.41–34.49)	29.8 ± 0.6 (27.66–31.96)	6.9 ± 0.7 (4.7–8.3)	1.33	3.92	3.41	3.2 ± 0.3 (summer)
Jul 2007	404 ± 6 (392–421)	366.7 ± 1.6 (362.6–370.8)	34.02 ± 0.12 (33.67–34.20)	30.3 ± 0.3 (29.09–30.96)	5.4 ± 0.5 (4.5–6.7)	1.30	3.51	3.06	
Oct 2003	355 ± 3 (349-359)	354.8 ± 0.9 (354.0–356.8)	34.11 ± 0.18 (33.65–34.44)	28.4 ± 0.3 (27.88–28.83)	9.2 ± 0.8 (6.8–10.8)	1.11	0.03	0.03	
Sep 2004	364 ± 3 (360–368)	357.7 ± 1.6 (354.7–361.0)	33.80 ± 0.14 (33.47–34.06)	28.8 ± 0.3 (28.45–29.30)	6.6 ± 1.2 (4.5–8.5)	1.38	0.96	0.84	
Oct 2006	369 ± 9 (345–385)	361.5 ± 1.2 (359.8–364.8)	33.73 ± 0.11 (33.28–33.90)	28.2 ± 0.3 (27.67–28.98)	8.1 ± 1.1 (4.9–9.9)	1.18	1.42	1.24	1.0 ± 1.8 (autumn)
Nov 2006	370 ± 5 (358–380)	370.0 ± 1.7 (366.9–374.0)	33.84 ± 0.10 (33.63–34.10)	26.8 ± 0.5 (25.35–27.50)	8.2 ± 0.7 (6.4–9.7)	1.31	−0.07	−0.06	
Sep 2007	394 ± 8 (376–411)	364.0 ± 0.8 (361.6–365.1)	33.21 ± 0.14 (32.82–33.39)	29.7 ± 0.5 (28.60–30.40)	6.5 ± 0.4 (5.5–7.7)	1.55	4.83	4.20	

* The average of field-measured values in November 2006 in domain B and during 22–23 December 2006 in domain A (Table 3).

BGD
10, 7031–7074, 2013

Seasonal variations of air-sea CO_2 fluxes in the South China Sea

W.-D. Zhai et al.

Table 5. Summary of pCO_2, salinity and SST along cruise tracks, monthly satellite-derived wind speed, and sea–air CO_2 flux estimation in domain C. *C*2 and most errors in sea–air CO_2 flux estimation are the same as in Table 3. In winter, however, the error presented here was estimated based on the standard deviation of the wind speed, since only one cruise was available in this season. See texts for details.

Observation time	Aqueous pCO_2 µatm	Air pCO_2 µatm	Salinity psu	SST °C	Wind speed $m\,s^{-1}$	*C*2	Sea–air CO_2 fluxes ($mmol\,CO_2\,m^{-2}\,d^{-1}$) Survey average (W92)	Survey average (S07)	Seasonal average
1–11 Dec 2006	383 ± 5 (368–404)	No data (375*)	33.42 ± 0.19 (33.03–33.89)	27.7 ± 1.3 (24.14–28.96)	10.2 ± 1.4 (6.0–12.3)	1.12	2.18	1.90	1.9 ± 0.5 (winter)
May 2004	386 ± 7 (360–405)	356.5 ± 2.2 (350.9–362.8)	33.77 ± 0.15 (33.19–34.31)	29.6 ± 0.5 (27.65–30.65)	5.6 ± 0.5 (4.0–7.2)	1.38	3.10	2.70	2.8 ± 0.2 (spring)
Apr 2005	412 ± 14 (383–463)	366.7 ± 2.2 (362.6–373.6)	33.89 ± 0.15 (33.48–34.33)	28.5 ± 0.4 (27.47–29.63)	5.1 ± 0.6 (4.1–7.6)	1.21	3.42	3.00	
Jul 2007	404 ± 6 (393–415)	366.9 ± 2.1 (364.7–370.5)	34.02 ± 0.09 (33.70–34.11)	30.2 ± 0.3 (29.73–30.82)	6.6 ± 1.1 (4.4–9.1)	1.42	5.64	4.91	6.6 ± 2.4 (summer)
Aug 2007	410 ± 14 (380–440)	364.5 ± 2.4 (360.5–369.3)	33.68 ± 0.24 (32.44–34.04)	28.3 ± 0.8 (25.89–30.25)	8.1 ± 1.3 (1.4–10.6)	1.30	9.58	8.35	
Oct 2003	367 ± 9 (350–385)	354.7 ± 3.1 (349.1–361.6)	33.26 ± 0.47 (32.09–34.36)	29.4 ± 0.8 (27.58–30.47)	6.9 ± 1.2 (4.6–10.2)	1.35	1.85	1.62	3.7 ± 2.9 (autumn)
Sep 2007	404 ± 10 (376–436)	364.1 ± 3.8 (358.3–375.5)	32.49 ± 0.61 (30.56–33.68)	29.3 ± 0.7 (28.09–30.37)	6.7 ± 1.2 (4.2–11.5)	1.53	6.59	5.74	

* The average of field-measured values between November 2006 and 22–23 December 2006 in domain A (Tables 3).

BGD
10, 7031–7074, 2013

Table 6. Summary of pCO_2, salinity and SST along cruise tracks, monthly satellite-derived wind speed, and sea–air CO_2 flux estimation in domain D. $C2$ and the error in sea–air CO_2 flux estimation in winter are the same as in Table 3. In the other seasons, however, the errors were estimated based on the standard deviation of the aqueous pCO_2 which primarily represented the spatial variation of aqueous pCO_2, since only one cruise was available in every season. See texts for details.

Observation time	Aqueous pCO_2 µatm	Air pCO_2 µatm	Salinity psu	SST °C	Wind speed $m\,s^{-1}$	$C2$	Sea–air CO_2 fluxes ($mmol\,CO_2\,m^{-2}\,d^{-1}$) Survey average (W92)	Survey average (S07)	Seasonal average
15–16 Dec 2006	367 ± 5 (357–379)	No data (375[a])	33.97 ± 0.17 (33.74–34.37)	25.2 ± 0.4 (24.55–25.83)	12.4 ± 1.0 (8.9–14.6)	1.05	−3.15	−2.74	11.0 ± 13.8 (winter)
21–22 Dec 2006	410 ± 20 (379–469)	375.4 ± 2.9 (372.2–382.2)	34.01 ± 0.24 (33.50–34.47)	25.0 ± 0.9 (23.58–27.08)	17.9 ± 2.1[b] (11.4–22.3)	1.04[b]	28.5	24.8	
Apr 2008	370 ± 13 (355–397)	378.6 ± 2.2 (374.0–382.7)	34.04 ± 0.13 (33.66–34.28)	27.9 ± 0.4 (26.82–28.72)	6.5 ± 0.8 (4.6–8.8)	1.34	−1.24	−1.08	−1.1 ± 1.5 (spring)
Jul 2007	400 ± 6 (364–417)	366.5 ± 1.6 (363.5–370.4)	33.92 ± 0.16 (33.26–34.18)	30.3 ± 0.4 (29.38–31.65)	5.1 ± 0.4 (4.3–6.9)	1.38	2.95	2.57	2.6 ± 0.4 (summer)
Sep 2004	361 ± 3 (354–366)	356.8 ± 1.7 (354.2–359.9)	33.78 ± 0.22 (33.47–34.23)	28.9 ± 0.3 (28.41–29.50)	7.5 ± 0.5 (6.4–9.7)	1.39	0.86	0.74	0.7 ± 0.5 (autumn)

[a] The average of field-measured values during 21–22 December 2006.

[b] Based on field-measured wind speeds at 10 m height by the onboard weather station along the survey transect.

BGD
10, 7031–7074, 2013

Seasonal variations of air-sea CO_2 fluxes in the South China Sea

W.-D. Zhai et al.

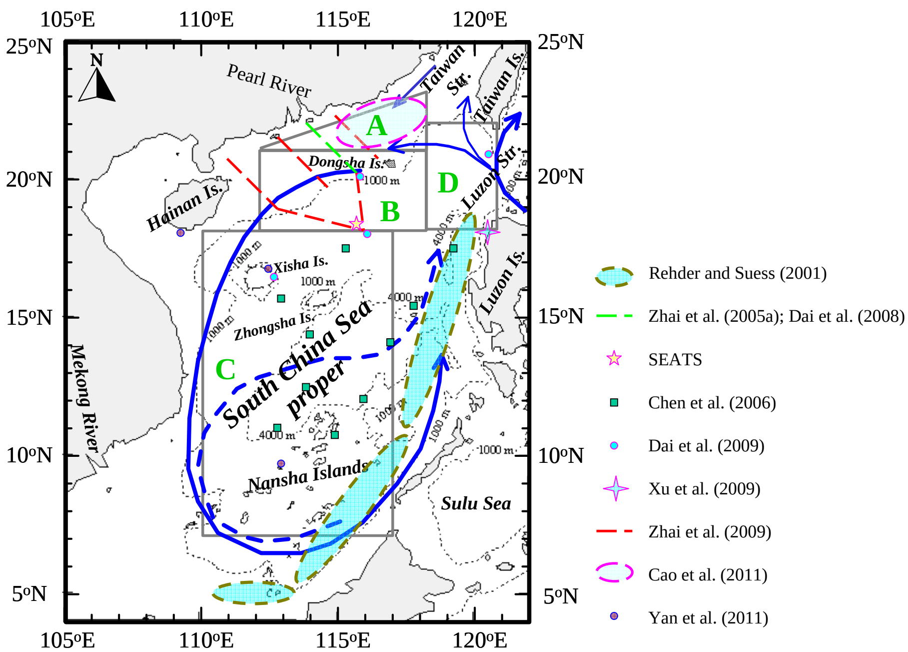

Fig. 1. Map of the South China Sea (SCS) area under study. Framed areas indicate the four physical-biogeochemical domains this study categorized, as detailed in Table 1. Blue curves represent the basin wide cyclonic gyre in winter (solid curve in the SCS) and the anticylonic gyre over the southern half of the sea during the summer (dashed curve in the SCS) and the Kuroshio and its intrusions (solid curves around the Luzon Strait) into the northern SCS. All published research related to air–sea CO_2 fluxes in the SCS are summarized (see the text for details). Note that the air–sea CO_2 flux at the SEATS station is well studied in Chou et al. (2005), Tseng et al. (2007), and Sheu et al. (2010b).

BGD
10, 7031–7074, 2013

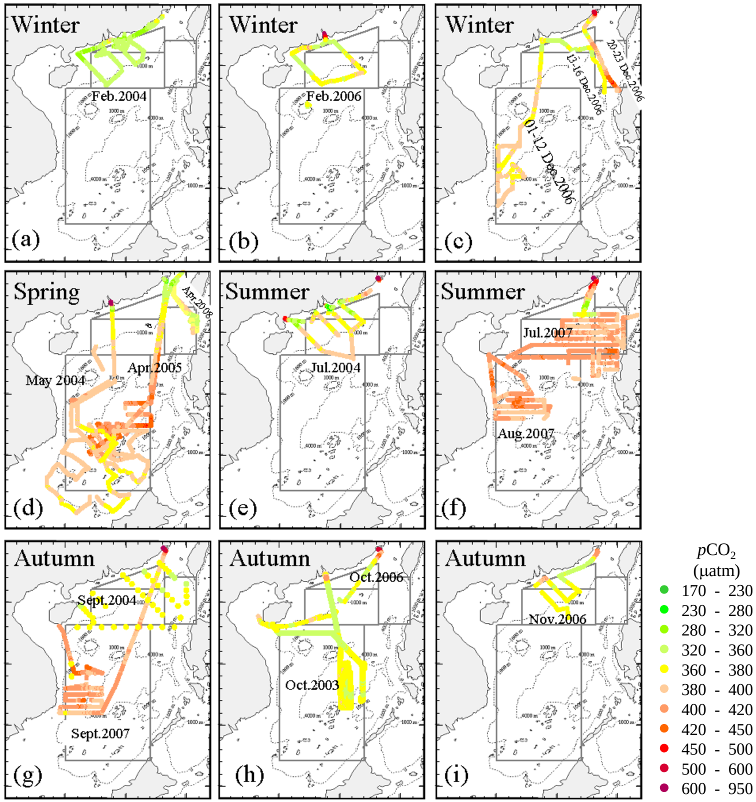

Fig. 2. Spatial distribution of sea surface pCO_2 during seasonal surveys conducted between October 2003 and April 2008.

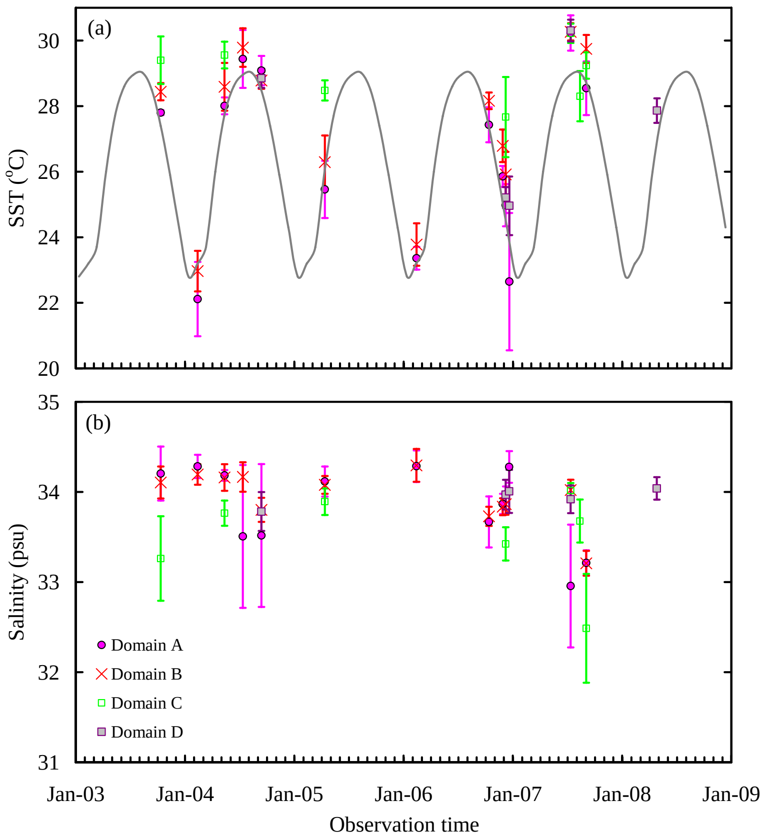

Fig. 3. Time series of **(a)** field-measured sea surface temperature (SST) and **(b)** salinity (mean ± standard deviation). In panel **(a)**, long-term monthly mean SST (NODC_WOA98 data, http://www.esrl.noaa.gov/psd/) at the position of 20° N 116° E is plotted as a grey curve.

BGD
10, 7031–7074, 2013

Seasonal variations of air-sea CO_2 fluxes in the South China Sea

W.-D. Zhai et al.

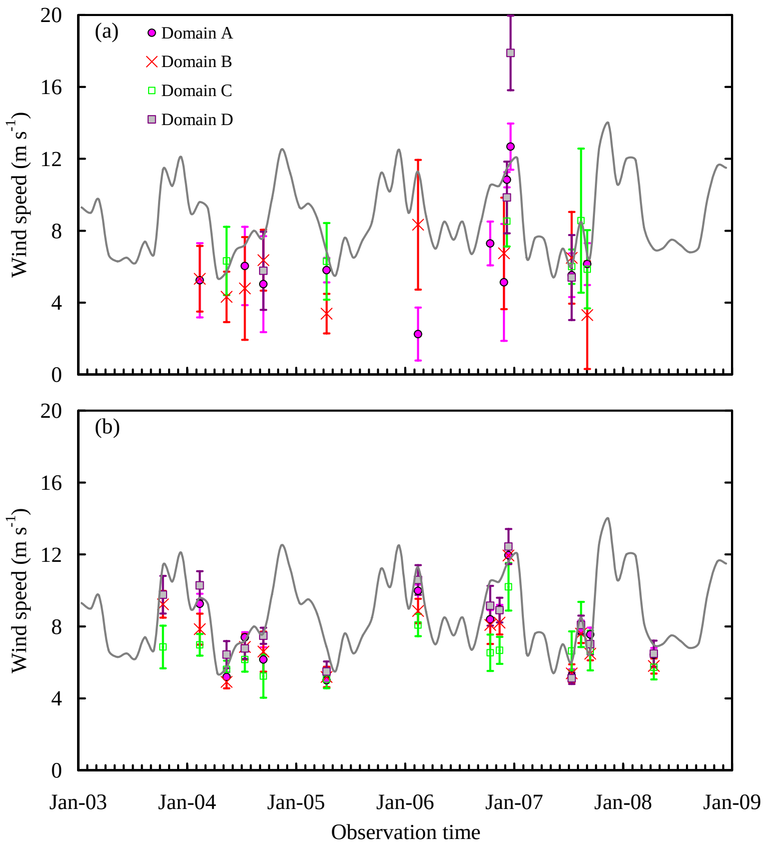

Fig. 4. Field-measured wind speeds at 10 m height **(a)** and monthly satellite-derived sea surface wind speeds **(b)** (QuikSCAT, Level 3). Data are shown as mean±standard deviation. The NCEP monthly mean sea surface wind speed (http://www.esrl.noaa.gov/psd/) at 20° N 116° E is plotted as a grey curve.

BGD
10, 7031–7074, 2013

Seasonal variations of air-sea CO_2 fluxes in the South China Sea

W.-D. Zhai et al.

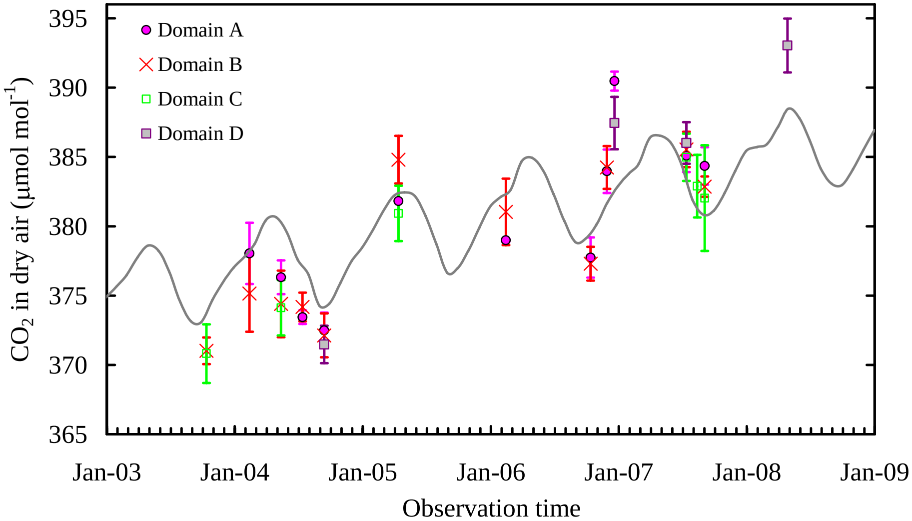

Fig. 5. Time series of field-measured CO_2 in dry air (mean ± standard deviation) during October 2003 to April 2008. A monthly mean data set for the Mauna Loa station (NOAA/ESRL, www.esrl.noaa.gov/gmd/ccgg/trends/) is also plotted as a grey curve.

BGD
10, 7031–7074, 2013

Seasonal variations of air-sea CO_2 fluxes in the South China Sea

W.-D. Zhai et al.

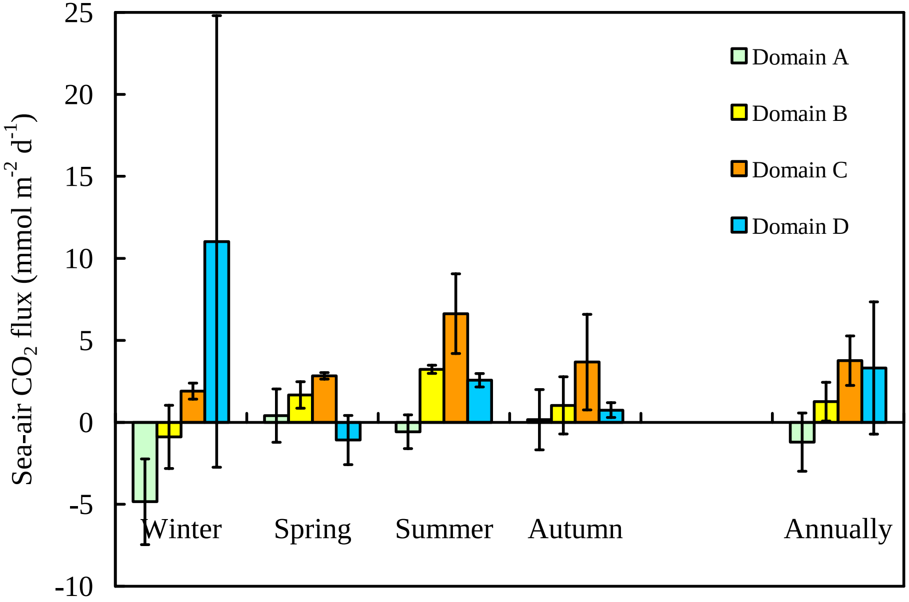

Fig. 6. Sea–air CO_2 flux estimation in the biogeochemical domains in the South China Sea proper.

BGD

10, 7031–7074, 2013

Seasonal variations of air-sea CO_2 fluxes in the South China Sea

W.-D. Zhai et al.

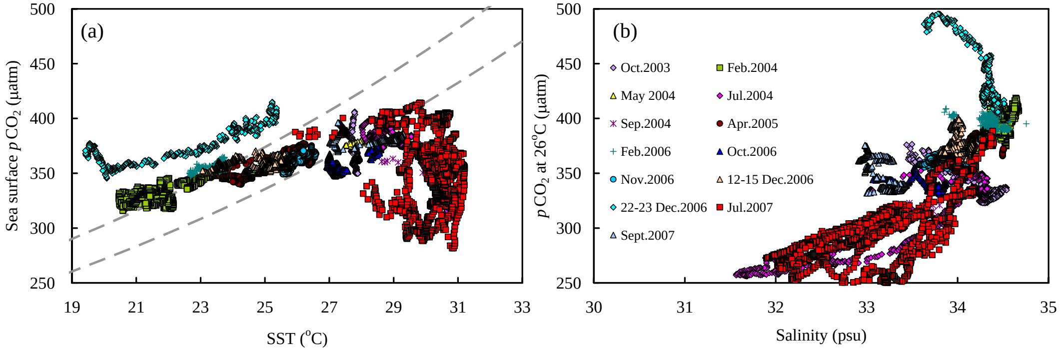

Fig. 7. Scatter plots of $p\mathrm{CO_2}$ as a function of temperature **(a)** and temperature normalized $p\mathrm{CO_2}$ versus salinity **(b)** in domain A. Dashed lines in panel **(a)** represent functions of $p\mathrm{CO_2}\,(\mu\mathrm{atm}) = 390 \times e^{0.0423(\mathrm{SST}-26)}$ (the upper line) and of $p\mathrm{CO_2}\,(\mu\mathrm{atm}) = 350 \times e^{0.0423(\mathrm{SST}-26)}$ (the lower line) according to Zhai et al. (2005a).

BGD
10, 7031–7074, 2013

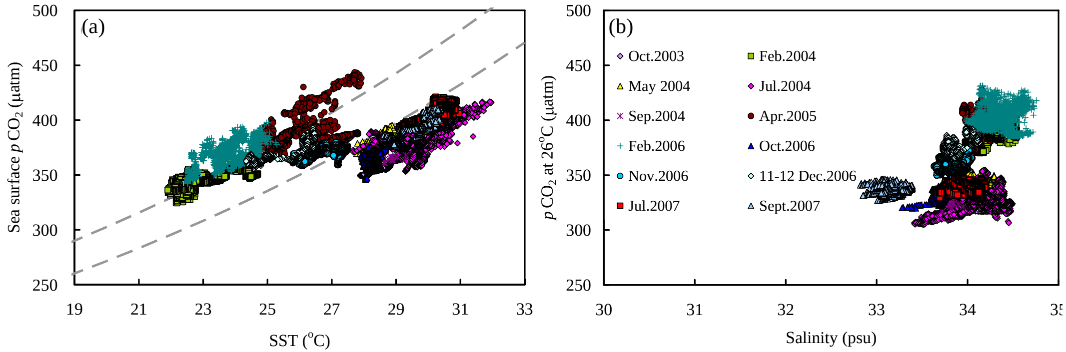

Fig. 8. Scatter plots of pCO_2 as a function of temperature **(a)** and temperature normalized pCO_2 versus salinity **(b)** in domain B. Dashed lines in panel **(a)** are the same as in Fig. 7a.

BGD
10, 7031–7074, 2013

Seasonal variations of air-sea CO_2 fluxes in the South China Sea

W.-D. Zhai et al.

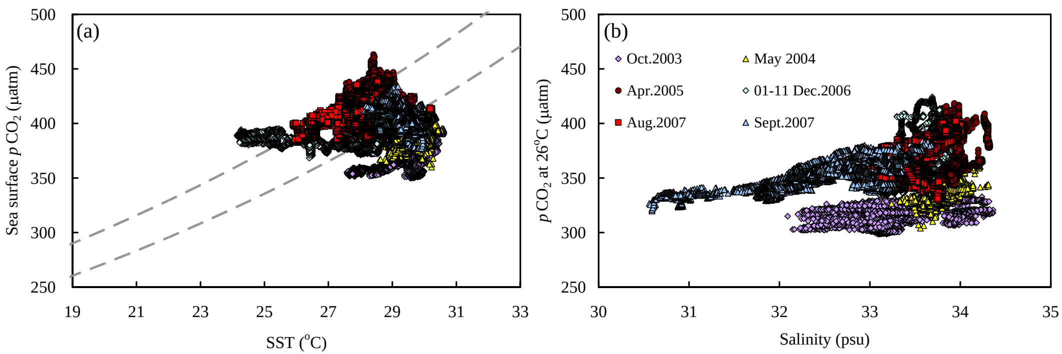

Fig. 9. Scatter plots of pCO_2 as a function of temperature **(a)** and temperature normalized pCO_2 versus salinity **(b)** in domain C. Dashed lines in panel **(a)** are the same as in Fig. 7a.

BGD
10, 7031–7074, 2013

Seasonal variations of air-sea CO_2 fluxes in the South China Sea

W.-D. Zhai et al.

Title Page
Abstract | Introduction
Conclusions | References
Tables | Figures
◂◂ | ▸▸
◂ | ▸
Back | Close
Full Screen / Esc
Printer-friendly Version
Interactive Discussion

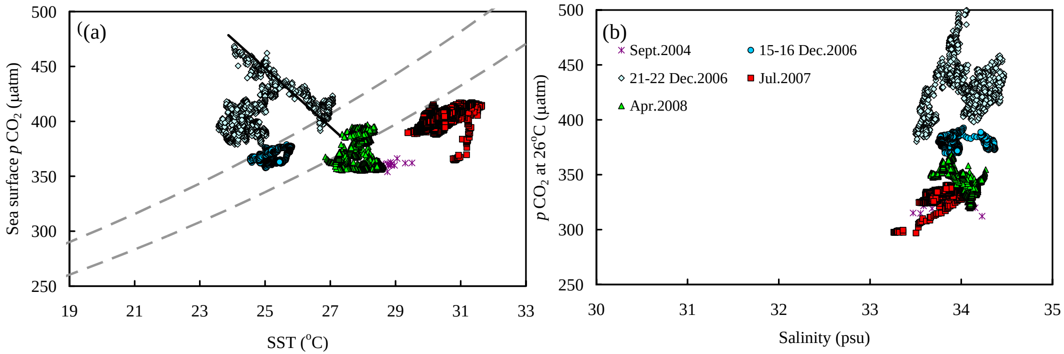

Fig. 10. Scatter plots of pCO_2 as a function of temperature **(a)** and temperature normalized pCO_2 versus salinity **(b)** in domain D. In panel **(a)**, dashed lines are the same as in Fig. 7a, while the real line represents a function of $pCO_2\,(\mu\text{atm}) = -26.737 \times \text{SST}\,(^\circ\text{C}) + 1116.9$ obtained during a neighboring research on 18–20 December 2006 according to Xu et al. (2009).

BGD
10, 7031–7074, 2013

W.-D. Zhai et al.

Title Page
Abstract | Introduction
Conclusions | References
Tables | Figures
◀| |▶
◀ ▶
Back | Close
Full Screen / Esc
Printer-friendly Version
Interactive Discussion